Electromigration in dilute body-centred cubic alloys

1998 J. Phys.: Condens. Matter 10 6687

(http://iopscience.iop.org/0953-8984/10/30/009)

J. Phys.: Condens. Matter **10** (1998) 6687–6706. Printed in the UK PII: S0953-8984(98)91573-9

Electromigration in dilute body-centred cubic alloys

J P Dekker† and A Lodder

Faculteit Natuurkunde en Sterrenkunde, Vrije Universiteit, De Boelelaan 1081, 1081 HV Amsterdam, The Netherlands

Received 11 February 1998, in final form 19 May 1998

Abstract. A multiple-scattering theory for the wind force in dilute substitutional alloys is applied as an *ab initio* method to body-centred cubic (BCC) metals. Results are given for self-electromigration in the alkali metals and the group IIA, IVA, VA and VIA metals. For many transition metal systems, the wind force is found to point in the direction of the electric field, which is in agreement with experiment and which could not be reproduced by simpler electronic structure models used in the past. The specific role of the vacancy in the scattering process, leading to the wind force at the initial position of a migrating atom, is made explicit for the group VA metal V. Migration of 3d, 4d and 5d impurities in the metals V, Nb and Ta is studied systematically.

1. Introduction

Electromigration occurs when a metal is subjected to an electric field. The random diffusive motion of atoms then gets a preferential direction. The force on an atom induced by the electric field consists of two components, the direct force and the wind force. The direct force is due to a net charge of the moving atom, while the wind force is due to scattering of the current-carrying electrons off the atom. Both forces are proportional to the electric field and can be characterized by a valence:

$$\boldsymbol{F} = (Z_{\text{direct}} + Z_{\text{wind}})e\boldsymbol{E} = Z^* e\boldsymbol{E}. \tag{1}$$

The effective valence Z^* is the measurable quantity. The *ab initio* quantum-mechanical calculation of the wind valence in BCC metals is the subject of this article.

Atoms can move in quite different ways, e.g. along the surface, along grain boundaries and inside the bulk. The mechanism that determines the atomic motion depends on temperature. In our calculations a monovacancy mechanism is assumed, which is supposed to prevail at high temperatures [1]. So, an atom moves by jumping from an initial lattice position towards a neighbouring vacancy. The atom has to overcome an energy barrier with its top halfway along the jump path, at the so-called saddle-point position. The wind force will be calculated at all positions along the path.

Obviously, in order to calculate this force, which is due to scattering of electrons, the electron wave function has to be known. The electron wave function of the dilute alloy $\Psi_k(\boldsymbol{r})$ is calculated from the electron wave function in the unperturbed host using a Green's function formalism, described by Dekker *et al* [2] and going back to the theory given by Lodder [3, 4]. In this formalism, the local modifications of the electronic structure at and around the migrating atom are accounted for exactly. The host wave function is calculated

† Present address: Max-Planck-Institut für Metallforschung, Seestrasse 92, D-70174 Stuttgart, Germany.

0953-8984/98/306687+20$19.50

using the Korringa–Kohn–Rostoker (KKR) method [5, 6]. The alloy wave function is used to calculate the wind force on an atom located at a position $\boldsymbol{R}_p$ along the migration path, from the quantum-mechanical expression given by Sorbello *et al* [7]

$$\boldsymbol{F}_{\text{wind}}(\boldsymbol{R}_p) = -\int \delta n(\boldsymbol{r})\, \boldsymbol{\nabla}_{\boldsymbol{R}_p} v_p(\boldsymbol{r} - \boldsymbol{R}_p)\ \mathrm{d}^3 r = \sum_k \delta f(k)\, \langle \Psi_k | -\boldsymbol{\nabla}_{\boldsymbol{R}_p} v_p | \Psi_k \rangle \tag{2}$$

which dates back to the pioneering work of Bosvieux and Friedel [8], and in which v_p is the potential of the migrating atom. The right-hand side of equation (2) makes explicit how the locally perturbed electronic density $\delta n(\boldsymbol{r})$ is composed of the density of electron states labelled by the band indices $k = (n, \boldsymbol{k})$, and weighted by the deviation $\delta f(k)$ from the equilibrium Fermi–Dirac distribution function. The important ingredients of the theory are summarized in section 2.

Results for self-electromigration, i.e. electromigration of host atoms, in the group VA metals V, Nb and Ta are given in section 3. A closer look at the scattering processes is taken for vanadium in section 4. Impurity migration in the group VA metals is considered in section 5. In this section the calculated wind valences of three series of transition metal atoms are presented. In section 6 results are presented for other BCC metals, namely for self-electromigration in the alkali metals and the group IIA, IVA and VIA metals. The results are summarized in section 7.

Throughout the article, atomic units are used, such that $\hbar = 2m = 1$. Exceptions are stated explicitly.

2. Theory

First we want to highlight the complexity of the electromigration problem, which can be illustrated nicely by looking at equation (2). It contains two different ingredients, one requiring the treatment of a local scattering problem, and another one requiring the solution of the electronic transport problem. Locally, one has to evaluate the matrix element of the force operator $-\boldsymbol{\nabla}_{\boldsymbol{R}_p} v_p$, to which end the electronic structure problem, which is an equilibrium problem, has to be solved. The transport problem is usually handled by solving Boltzmann's equation, whereby the occupation of the electron states is obtained. This can be written as the sum of the equilibrium Fermi–Dirac distribution function $f_0(k)$ and the deviation $\delta f(k)$ due to the presence of an electric field $\boldsymbol{E}$. Since $f_0(k)$ obviously leads to a zero contribution to the electric current in the system, and so also to the 'wind', only $\delta f(k)$ appears in equation (2). The progress made relates to the local problem. Looking back in history, it can be seen that the progress has been very slow. Besides the free-electron-model treatment by Bosvieux and Friedel [8], for many years the model-pseudopotential treatment proposed by Sorbello [9] was the only available one, and this was applicable to simple metals and weakly scattering impurities only. The first realistic treatment is due to Gupta [10]; this was based on multiple-scattering theory. As regards the evaluation of the wind force at an arbitrary position of the migrating atom along its jump path, Gupta's treatment was still approximate, which was illustrated most clearly by the formulation of the full theory published somewhat later [3]. That is probably why Gupta restricted consideration to just a few applications [10, 11]. The solution of the problems involved has been presented only recently [12, 13]. The first complete results were obtained for a series of FCC metals [2]. In the present paper a great number of BCC metals will be treated.

Before this could be done, other approximate calculations were made, starting from the full theory, but treating only the local electronic scattering problem rigorously [14, 15]. The correct host environment of the electromigration defect, which can now be accounted

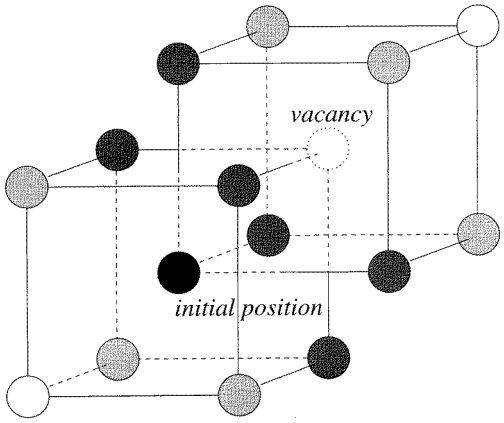

Figure 1. A cluster of 16 atoms along and near the path from an initial position to a neighbouring vacancy, forming the electromigration defect. For the BCC structure shown, the path lies in the (111) direction. The various grey colours are meant to indicate that at least 14 of these atoms are perturbed host atoms. The cluster is supposed to be embedded in a pure host.

for, was at that time replaced by free space. Figure 1, to which we return at the end of this section, shows an example of such a substitutional electromigration defect in a BCC crystal. Free electrons were multiply scattered by the atomic potentials forming the cluster, and locally exact wave functions were used to calculate the wind force on an atom in such a cluster. The results were unexpected and astonishing. For certain transition metals the wind force on hydrogen [14] and on an atom at a substitutional position [15] was found to point in the direction of the electric field. This was in agreement with experiment, but a naive picture would require hole conduction to be dominant in order to obtain such a result. Since no holes are present in a finite-cluster description of a solid, the Fermi surface, let alone details of it, is apparently not important, and the old naive picture broke down for electromigration in metals. However, such model results remain dependent on the cluster size to too great an extent [15], and the measured negative Z_{wind} for hydrogen in tantalum could not be reproduced [14, 16]. Therefore, embedding of the cluster in the complete host matrix remains important, as regards both the magnitude and the direction of the wind force.

The expressions to be calculated numerically have been derived in the framework of multiple-scattering theory. Within the muffin-tin approximation for the system potential, which has been shown to be a good approximation for electromigration of hydrogen in FCC and BCC metals [16], these expressions are exact. The individual atomic scatterers, the potentials of which are constructed from atomic charge densities calculated *ab initio*, enter the theory via their phase shifts at the Fermi energy. From this one derives from equation (2) the following expression [3]:

$$\boldsymbol{F}_{\mathrm{wind}}(\boldsymbol{R}_p) = -2e\tau\,\mathrm{Re}\sum_{L}\sum_{m_1=-(l+1)}^{l+1}\boldsymbol{D}_{L;l+1,m_1}\sin(\eta_{l+1}-\eta_l)\mathrm{e}^{\mathrm{i}(\eta_{l+1}-\eta_l)}\boldsymbol{V}^{p}_{L;l+1,m_1}\cdot\boldsymbol{E}. \tag{3}$$

One sees that this expression is proportional to the electron transport relaxation time τ of the system, to the vectorial Gaunt coefficients

$$\boldsymbol{D}_{LL'} = \int \mathrm{d}\hat{\boldsymbol{x}}\; Y_L(\hat{\boldsymbol{x}})\hat{\boldsymbol{x}}Y_{L'}(\hat{\boldsymbol{x}}) \tag{4}$$

which originate from the space integral in equation (2) and where $\hat{\boldsymbol{x}}$ stands for the unit

vector in the $\boldsymbol{x}$-direction, to the vectorial integral $\boldsymbol{V}$ over the Fermi surface (FS)

$$\boldsymbol{V}^p_{LL'} = -\frac{2}{\Omega_{\mathrm{BZ}}} \int_{\mathrm{FS}} \mathrm{d}S_k \; c_{kpL} \hat{\boldsymbol{v}}_k c_{kpL'} \tag{5}$$

which originates from the summation over k in equation (2), and to the electric field $\boldsymbol{E}$, while the phase shifts η for the different angular momenta $L = (l, m)$ represent the potential v_p of the migrating atom. Note that only phase shifts couple with $\Delta l = 1$, which comes from the gradient operator in equation (2).

The quantities τ, $\boldsymbol{V}$, and the field $\boldsymbol{E}$ come from $\delta f(k)$, which is proportional to $\tau_k \boldsymbol{v}_k \cdot \boldsymbol{E}$, while τ_k has been replaced by an average isotropic value, as has always been done in electromigration theory. Since τ determines the current density, which is an average quantity as well, and a value for it is derived from the sample resistivity taking into account an integration over the Fermi surface [16], this approximation is not expected to have serious consequences. The magnitude of the wind force, and particularly its direction—whether it is directed parallel or oppositely to the electric field direction—have proven to be much more sensitive to the local scattering aspects, covered by the vector $\boldsymbol{V}$ and the phase shifts η, which require an accurate account of the electronic structure [16]. The electron velocity $\boldsymbol{v}_k$ is present in the quantity $\boldsymbol{V}$, and is extracted from the electronic structure of the host metal. The alloy wave-function coefficients c_{kpL} enter straightforwardly, on using the representation

$$\Psi_k(\boldsymbol{x} + \boldsymbol{R}_p) = \sum_L c_{kpL} R^p_L(\boldsymbol{x}) \tag{6}$$

in which $R^p_L(\boldsymbol{x})$ is the locally exact partial wave solution of the Schrödinger equation for the potential v_p. The alloy wave-function coefficients are related to those of the host by a matrix, which accounts for all of the backscattering of outgoing waves from the electromigration defect by the host environment and is given by Dekker *et al* [2]. This matrix, which was replaced by the unity matrix in Gupta's work, contains the host Green's function matrix, the evaluation of which forms the difficult part of the problem from a computational point of view [12]. The host wave-function coefficients are calculated routinely using the KKR method for the host band structure [5, 6].

Now we want to discuss the consequences of three features of equation (3), namely that the wind force is proportional to the transport relaxation time τ, that its direction is not necessarily parallel to the electric field $\boldsymbol{E}$ and that the wind force is position dependent. The proportionality of the wind force to τ implies that the wind force and, consequently, the wind valence are inversely proportional to the sample resistivity ρ. If the wind valence is multiplied by the resistivity, a temperature-independent quantity K remains:

$$K = \rho Z_{\mathrm{wind}}. \tag{7}$$

Since results for Z_{wind} require a specification of the temperature, in many cases the quantity K will be given instead. As regards the magnitude of the sample resistivity, we want to point out that electromigration experiments are done at and way above room temperature, and the systems are supposed to be dilute alloys. Therefore the resistivity contribution of the impurities is small, and it can be considered as legitimate to use the host phonon resistivity as a measure for τ in equation (3) and for ρ in equation (7). As far as units are concerned, both ρ and K will be expressed in $\mu\Omega$ cm.

The direction of $\boldsymbol{F}_{\mathrm{wind}}$ is determined by the vector $\boldsymbol{D}$, which, in general, is not aligned with the electric field. The wind valence is a tensor built up out of the vectors $\boldsymbol{D}$ of

equation (4) and $\boldsymbol{V}$ of equation (5). For the symmetry of the assumed straight path in the BCC structure, the wind force can be written as

$$\boldsymbol{F}_{\text{wind}} = \frac{K_{\parallel}}{\rho} e\boldsymbol{E}_{\parallel} + \frac{K_{\perp}}{\rho} e\boldsymbol{E}_{\perp} \tag{8}$$

where $\boldsymbol{E}_{\parallel}$ and $\boldsymbol{E}_{\perp}$ are the components of the electric field parallel and perpendicular to the migration path. So, the wind force is parallel to the electric field only if the electric field is either parallel or perpendicular to the migration path and if, by chance, $K_{\parallel} = K_{\perp}$. In all other cases it is not. This will be discussed further in sections 4 and 5. For electromigration, which is an atomic transport process, only the component $K_{\parallel}$ is important. This becomes clear if one realizes that atomic transport arises from the work done by the force. In the cases in which only $K_{\parallel}$ is considered, it will be indicated simply by K.

The position dependence of the wind force is not measurable. In electromigration measurements the path average is probed, corresponding to the work done by the force during the jump, divided by the path length. It is convenient to indicate the position dependence by a path parameter s, which runs from 0 to 1 in moving $\boldsymbol{R}_p$ from the initial position to the final position along the jump path, as a result of which the path average becomes an integral over s from 0 to 1. The path-averaged K shows up in the expression for the measurable effective valence:

$$Z^* = Z_{\text{direct}} + \frac{K}{\rho}. \tag{9}$$

Since the variation over the path can be considerable, we will display it figures 2, 12 and 13—see later.

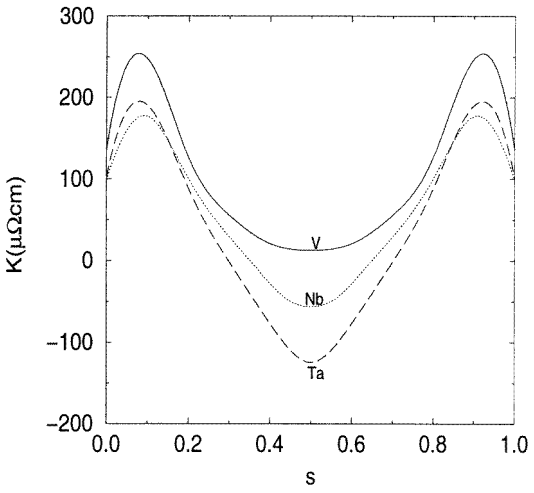

Figure 2. The variation along the migration path of the wind valence quantity K—see equation (9)—for self-electromigration in V, Nb and Ta. A positive K indicates that the wind force is in the direction of the electric field $\boldsymbol{E}$.

Finally, the locally perturbed electromigration defect region is depicted in figure 1. The host atoms surrounding the jump path are perturbed because of the presence of the vacancy and the impurity. As far as charge transfer is concerned, this perturbation is indicated symbolically by using different shades of grey for the different atoms. Lattice distortion effects are not large, provided that the correct self-consistent charge neutrality is taken care

of, which in our work is controlled by a generalized Friedel sum rule. The full cluster of 16 perturbed atoms is taken into account.

Table 1. Z_{wind} for V, Nb and Ta at $0.9T_{\mathrm{m}}$, the resistivities at $0.9T_{\mathrm{m}}$ and at 2000 K, and the melting temperature T_{m}.

	$Z_{\mathrm{wind}}(0.9T_{\mathrm{m}})$	$\rho(0.9T_{\mathrm{m}})$ ($\mu\Omega$ cm)	ρ(2000 K) ($\mu\Omega$ cm)	T_{m}
V	0.99	105.5	107.2	2170
Nb	0.76	81.5	71.4	2743
Ta	0.35	106.9	78.9	3270

3. Self-electromigration in the transition metals V, Nb and Ta

The variation of K along the path is similar for each of the three group VA elements, as is shown in figure 2. In the figure s runs from 0 to 1, as the atom moves from its initial to its final position, so $s = \frac{1}{2}$ at the saddle point. Initially, an atom moving towards the neighbouring vacancy 'feels' a growing wind force in the direction of the electric field. This was already observed by van Ek *et al* [17] for Nb and was interpreted as indicating an average positive wind valence which is larger than the value at the initial position. However, if the calculation is extended over the entire path, it turns out that the wind force starts to reduce at some point and reaches a minimum at the saddle point, even being negative for Nb and Ta. The calculated average wind valences at a temperature of 90% of the melting temperatures are all positive and decrease with increasing atomic number as is shown in table 1. In this table, the melting temperature T_{m} and the resistivities at 0.9 T_{m} and at 2000 K are also given.

The wind valence for self-electromigration in Nb has already been calculated by Gupta *et al* [11], Brand and Lodder [15] and van Ek and Lodder [17], using different methods. The calculations of Gupta *et al* account for the electronic structure of the host, but important multiple-scattering effects, leading to a modification of the wave-function coefficients, are neglected. Brand and Lodder have used a finite-cluster model, which does account for multiple-scattering effects, but neglects the electronic structure of Nb. Our calculation can be viewed as an extension of the calculation of van Ek and Lodder, who account for both the multiple-scattering and the electronic structure, but who could only perform calculations near the initial position (up to 3% of the lattice constant).

Table 2. Calculated wind valences at 2300 K for self-electromigration in Nb in the initial position and at the saddle point, and the average over the path according to different authors.

	Initial position	Saddle point	Average
Gupta *et al* [11]	0.00	0.19	0.10
Brand and Lodder [15]	Not available	Not available	0.71
van Ek and Lodder [17]	1.33	Not calculated	—
Present work	1.25	−0.70	0.77

The average wind valences found by different authors are listed in table 2. The use of an unperturbed local host potential and the unperturbed Bloch wave function by Gupta *et al* leads to a zero wind valence at the initial position, so the average value is based

on the saddle-point wind valence of $+0.19$ at 2300 K. This value contradicts our negative value of -0.70 at 2300 K. The calculations of Brand and Lodder are interesting, because of the positive sign of the wind valence. The starting point of their calculation is a cluster in free space, in which the cluster size ranges from 4 to 18 atoms. The charge carriers are therefore electrons, which clearly move against the direction of the electric field. Nonetheless, they exert a scattering force on a Nb atom in the opposite direction. Moreover, the results obtained by Brand and Lodder compare well with ours, although they find a strong dependence on the cluster size. Their calculations illustrate the importance of multiple-scattering effects, which even seem to be more important than the effect of taking into account the correct electronic structure. Combining the measured effective valence at 2300 K given by Gupta *et al* [11] of 4.0 and our calculated wind valence of 0.8, one finds a direct valence of $+3.2$. This is reasonable in view of the chemical valence of $+5$.

Our calculated K-value together with the measured resistivity leads to a relatively weak temperature dependence of the wind valence: it varies from a value of 1.2 at 1300 K down to a value of 0.7 at T_m. However, Ernst *et al* [18] observed an effective valence varying from $+4.5$ at 1813 K to $+1.3$ at 2513 K. They attribute the high value at lower temperatures to a dislocation pipe diffusion mechanism, while only at high temperatures would a mono-vacancy mechanism, as assumed in our calculations, become dominant. Combining the effective valence of $+1.3$ and our calculated K-value leads to a small direct valence of $+0.5$, corresponding to large screening.

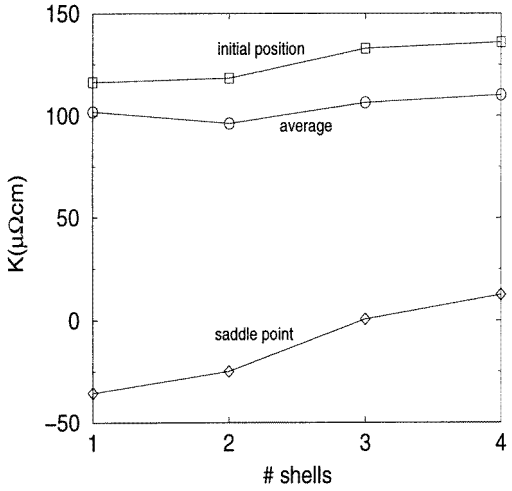

Figure 3. The quantity K at the initial and saddle-point positions, and the path-averaged value, as functions of the number of shells of perturbed atoms in V.

Similarly to the calculations by Brand and Lodder [15], our calculations are in principle dependent on the cluster size. However, we expect a much smaller dependence, because we account for the host embedment of the cluster, while the cluster of Brand and Lodder is embedded in free space. In the BCC structure, the largest cluster considered contains 16 host atoms, as shown in figure 1. This cluster consists of the nearest-neighbour shells of the initial position as well as the final position of the migrating atom. In this elongated structure, shells of atoms at the same distance from the saddle point can be defined. The first shell consists of the initial and final host positions. The initial position is indicated in figure 1 by a black circle, while the initial vacancy is indicated by a dotted circle. The

second shell consists of the six dark grey atoms, the third one of the six light grey atoms and the fourth one of the two white atoms.

Calculating K for all cluster sizes leads to profiles similar to those shown in figure 2. The maximum at about 10% of the migration path as well as the minimum at the saddle point are apparent. However, the precise values do change, as can be observed in figure 3 for V, in which K at the initial and saddle-point positions and its average over the path are given as functions of the number of shells. The average values lie between 96 and 110 $\mu\Omega$ cm—a variation of 13%. Although the cluster size dependence is not as pronounced as in the finite-cluster model, a noteworthy effect is apparent. If the cluster is enlarged, corresponding to an increasing number of perturbed host atoms, the sign of K at the saddle point changes from negative to positive for V. Apparently, charge transfer induces a reversal of the local current.

In the present work, the cluster size is chosen to encompass the full environment. Especially, when one looks into the detail of the electromigration process, this can be important. On the other hand, if the goal of the calculations is to get a feeling for the magnitude of the wind force, e.g. in order to analyse experimental data, a smaller cluster is sufficient.

4. The role of the vacancy

The wind valence at the initial position depends to a large extent on the presence of the vacancy. For self-electromigration this is most pronounced, because unperturbed host atoms do not scatter Bloch electrons. No vacancy, no wind force. The vacancy has two related effects. First, the absence of a host atom changes the potential of the surrounding host atoms, which is a charge-transfer effect as a result of which the host atom at its initial position becomes a real scatterer in contrast to a crystal host atom. Second, the vacancy scatters Bloch electrons and therefore also changes the wave function at a neighbouring host atom. We will study the two effects separately in more detail for a V host.

Table 3. The sp, pd and df contributions to K for a host vanadium atom next to a vacancy, using different potentials for the moving atom, the vacancy and the surrounding atoms. A perturbed host atom is indicated by V, an unperturbed atom by V^h. 'Vac' stands for 'vacancy'.

Moving atom	Vacancy site	Surrounding atoms	sp	pd	df	Total
V	Vac	V	9.1	178.4	−51.5	136.0
V	Vac	V^h	6.8	156.1	−46.5	116.4
V^h	Vac	V^h	6.0	171.4	−124.1	53.8
V	V^h	V^h	0.9	−21.0	105.6	85.0

The effect of charge transfer can be probed by calculating Z_{wind} for a perturbed host atom embedded in an otherwise perfect host. The second effect can be probed by calculating Z_{wind} for an unperturbed host atom next to a vacancy. In table 3 both effects of the vacancy on the sp, pd and df contributions to K are shown for a host V atom. The first column indicates which potential is used for the moving atom. This is either that for an unperturbed atom V^h or that for a perturbed host atom V. The second column indicates which potential is used at the position of the vacancy, which is either a vacancy ('Vac') potential or a V^h host potential. The third column indicates which potentials are used for the other neighbours of the vacancy, that for V^h or that for V. The first row contains the results for the realistic situation of a vacancy and a full nearest-neighbour shell of perturbed host

atoms. The pd term is relatively large and positive, while the df term is roughly one third as large and has the opposite sign. In the second row, all perturbed host atoms apart from the migrating one are replaced by host atoms. The relative magnitudes of the three contributions remain basically unchanged, but the absolute values are somewhat reduced. In the third row the moving atom is replaced by a host atom. The negative df contribution becomes considerably larger in magnitude, resulting in a much smaller wind force. The fourth row gives the scattering of Bloch electrons off a single atom affected by charge transfer and shows a completely different behaviour. The pd and df contributions change sign and the df contribution becomes dominant. The last rows probe the two effects mentioned, namely the effect of the vacancy as a scatterer and as a cause of charge transfer to or from the migrating atom. It can be concluded that these two effects of the vacancy are very different in character, but are equally important. The fact that the second row is not completely equal to the sum of the last two rows must be attributed to multiple-scattering effects.

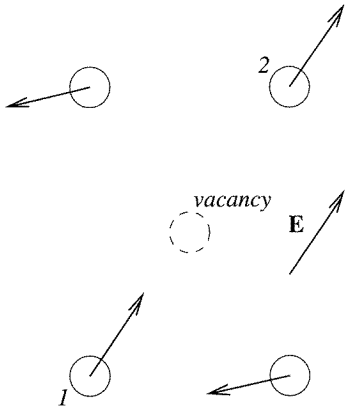

Figure 4. The wind force on atoms in a (110) plane, when $\boldsymbol{E}$ and the migration path of atom 1 are parallel.

Up to now we have only considered the component of the wind force directed along the migration path, which leads to a scalar wind valence and is the measurable component. It is interesting to study the full wind force. For the BCC structure this is given by equation (8), in which $K_{\parallel}$ is equal to the quantity K studied up to now. In figure 4 the wind force on four V atoms surrounding a vacancy in a (110) plane is shown. The field is parallel to the migration path of atom 1, so $\boldsymbol{E}_{\parallel} = \boldsymbol{E}$ and $\boldsymbol{E}_{\perp} = 0$. Because $K_{\parallel} > 0$, the force has the same direction as $\boldsymbol{E}$. Although the migration path of atom 2 is in the opposite direction, for symmetry reasons the force on this atom is equal to the force on atom 1, which is reproduced explicitly by our calculations. For the two other atoms, neither of the two components of the electric field is zero, and this leads to a force which is not parallel to the field. Such a strong spatial variation of the forces had already been observed by Sorbello [9].

A systematic picture of this variation is given in figure 5(a), which shows twelve different orientations of the crystal, obtained by clockwise rotation steps of 30° around the [110] axis. The direction of $\boldsymbol{E}$ has been chosen to be vertical. Rotation of $\boldsymbol{E}$ with respect to the jump path is depicted by rotating the jump path with respect to $\boldsymbol{E}$. The dot at position 1 corresponds to atom 1 in figure 4, and the vacancy is indicated by the dotted circle. The dot at position 2 shows atom 1 after rotation by 180°, and the force is equal to the force on

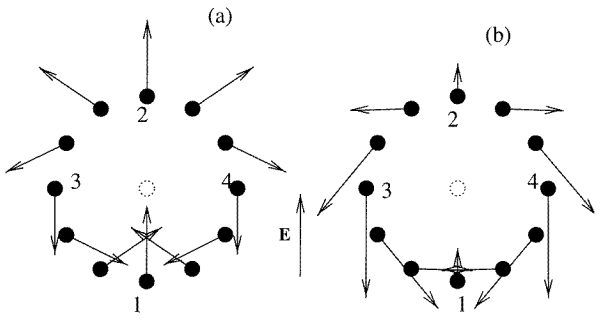

Figure 5. The wind force on atom 1 of figure 4, for different directions of the electromigration path with respect to the direction of the electric field $\boldsymbol{E}$. (a) The total wind force. (b) The component of the wind force due to the vacancy-induced current $\boldsymbol{j}_{\mathrm{scatt}}$.

atom 2 in figure 4. After clockwise rotation by an angle of 90°, atom 1 occupies position 3 and feels a force directed oppositely to the electric field, while its magnitude has been reduced by a factor of 0.86. So the wind force has reversed its direction, while the path has only rotated by 90°. After rotation by another 90°, the wind force has reversed its direction again, and points in the original direction for atom 1 at position 1.

How can this behaviour be interpreted? Let us adopt the simple intuitive picture of a wind force arising from the scattering of the local current of electrons $\boldsymbol{j}$ off the perturbed host potential. This current is composed of two components, the unperturbed sample current $\boldsymbol{j}_{\mathrm{sample}}$ to be considered as a constant input current, and a scattered current, to be denoted by $\boldsymbol{j}_{\mathrm{scatt}}$:

$$\boldsymbol{j} = \boldsymbol{j}_{\mathrm{sample}} + \boldsymbol{j}_{\mathrm{scatt}}. \tag{10}$$

The effect of $\boldsymbol{j}_{\mathrm{sample}}$ is already shown in the fourth row of table 3 and is represented by $K = K_{\parallel} = K_{\perp} = 85.0\ \mu\Omega$ cm. The separate effect of the residual $\boldsymbol{j}_{\mathrm{scatt}}$ is displayed in figure 5(b). The forces shown are obtained from the forces in the left-hand panel by subtracting the contribution due to $\boldsymbol{j}_{\mathrm{sample}}$. For a force proportional to the local current density, this picture suggests that $\boldsymbol{j}_{\mathrm{scatt}}$ consists of two circular currents. Both have the direction of $\boldsymbol{E}$ at the vacancy site. They bend back to the left and the right through the positions 3 and 4 respectively, where they have the opposite direction. Such a dipolar backflow was treated for a Fermi liquid by Pines and Nozières [19], while here it is found in a real solid. It is interesting to see the relation between figure 5 and the even earlier concept of the residual resistivity dipole as introduced by Landauer [20]. Using Sorbello's representation of it [21], the behaviour displayed in figure 5 is precisely reproduced, apart from an overall sign [22]. All of the force vectors point in the opposite direction, which is natural for a free-electron description of the host, as used in Landauer's picture. Given the field direction as in figure 5, the free-electron wind force on atom 1 at position 1 can point only oppositely to the field direction.

5. Systematic study of impurity migration in the group VA metals

The wind forces on 3d (Sc, Ti, V, Cr and Mn), 4d (Y, Zr, Nb, Mo and Tc) and 5d (La, Hf, Ta, W and Re) impurities in V, Nb and Ta are considered. Throughout this section, the wind forces are characterized by the temperature-independent quantity K. K can be converted

to a wind valence by making use of the resistivities, which are given for temperatures of 2000 K and 90% of the melting temperature in table 1 in section 3.

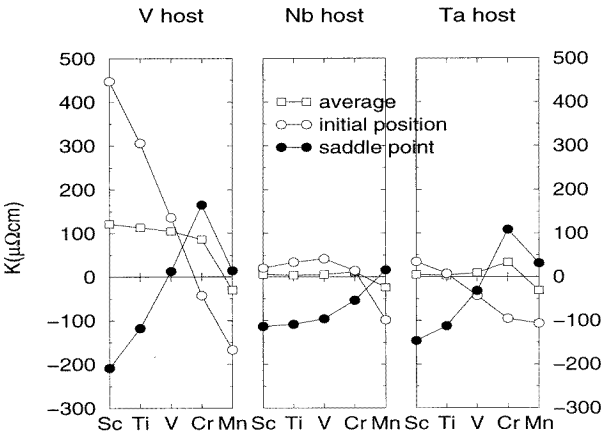

Figure 6. K for 3d impurities in V, Nb and Ta at the initial position and the saddle point, and the average over the path.

5.1. Migration of the 3d impurities Sc, Ti, V, Cr and Mn

In figure 6, results are given for the 3d impurities Sc, Ti, V, Cr and Mn in V, Nb and Ta. In addition to K averaged over the path, its values at the initial and saddle-point positions are shown. The average K, indicated by the squares, is almost constant as a function of the increasing atomic number of the impurities, apart from the solute Mn, which has a negative wind valence in all three hosts. In Nb and Ta hosts, the average wind valence of Cr is largest, while for V it decreases with the atomic number. Combining the K-values and the resistivities given by table 1 leads to wind valences of order 1 or smaller. In a Nb host, the wind valences at 2470 K (90% of T_m) range from -0.29 (Mn) to $+0.14$ (Cr) in this series. Measurement of the effective valence of these impurities in Nb and Ta could provide us with interesting information about the direct valence, which is the dominant contribution according to these calculations.

Although the average wind valence is almost independent of the kind of impurity in this series, the wind valences at the initial and saddle-point positions vary appreciably with atomic number. The wind valence at the initial position decreases as a function of the atomic number in both V and Ta. In Nb it increases up to V and decreases afterwards. This is striking, because V is electronically most similar to Nb. Therefore one would intuitively expect this impurity to scatter more weakly than other 3d impurities, leading to a lower K.

As regards the curves for the wind valence at the saddle point, those for Sc and Ti are negative, while the one for Mn is positive. Initially, the absolute values decrease with increasing atomic number. In Nb, the wind valence of Cr is still negative, while in V and Ta, it is positive and larger than that of Mn.

In section 4, the influence of the presence of the vacancy on host-atom migration has been investigated. A host atom does not feel a wind force if there is no vacancy next to it. In the case of an impurity atom this is different, because it is a scatterer anyway. But again, the presence of a vacancy next to it is expected to influence the strength of the force. This influence is shown in figure 7, where K for a single substitutional atom and $K_{\|}$ and

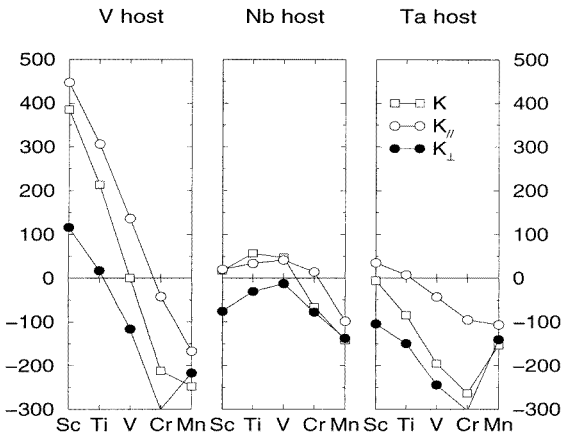

Figure 7. K for single 3d impurities compared to $K_{\parallel}$ and $K_{\perp}$ for 3d impurities next to a vacancy in V, Nb and Ta. The $K_{\perp}$-values for Cr in V and Ta are -301 and -303 respectively and are not marked. The open circles represent the same data as do the open circles in figure 6.

$K_{\perp}$ for an atom next to a vacancy are shown. K for all impurities in V and Ta considered, apart from Mn, lies between the values of $K_{\parallel}$ and $K_{\perp}$. This suggests an appealing intuitive explanation, which is triggered by the observed role of the vacancy in self-migration in section 3. The interaction between the single impurity and the sample current is reflected in K, which contributes to both $K_{\parallel}$ and $K_{\perp}$. The calculations in section 3 suggest that the vacancy induces a ring current of charge carriers, having the direction of $\boldsymbol{E}$ at the vacancy position. This current leads to a positive contribution to the measurable quantity $K_{\parallel}$ and a negative one to $K_{\perp}$.

The calculations for V and Ta hosts are consistent with the interpretation that the wind force on an impurity is generated mainly by separate interactions with $\boldsymbol{j}_{\text{sample}}$ and $\boldsymbol{j}_{\text{scatt}}$, where the scattered current arises from the presence of the vacancy. However, this linear picture may easily break down, because two relatively strong scatterers are next to each other. This may be the case in Nb, in which the vacancy does not induce a positive contribution to $K_{\parallel}$ and a negative one to $K_{\perp}$ for all impurities. For Sc, Ti and V, K approximately equals $K_{\parallel}$, and for Cr and Mn, it approximately equals $K_{\perp}$. This indicates either another effect of the vacancy in Nb or a larger interaction between the vacancy and the impurity. Mn shows a different behaviour in all of the hosts. K for a single Mn atom has a larger negative value than either $K_{\parallel}$ or $K_{\perp}$.

Another interesting question is raised by the opposite signs of K for the single impurities Sc and Ti on the one hand and for Cr and Mn on the other hand, both in V. Intuitively, one would expect the sign of K to be determined by the direction of the motion of the charge carriers, which is determined by the host and not by the impurity. The wind force on an atom in free space is indeed in the direction of motion of the charge carriers. Therefore the explanation has to be found by considering the crystal environment.

Backscattering can be part of the explanation. The qualitative picture of this is relatively simple. A Bloch wave reaches the impurity without being scattered, because it has only passed host atoms. This wave is scattered by the impurity, which gives rise to a wind valence, the sign of which is determined by the direction of the charge carriers. If this were to be the end of the story, the difference in sign of K for Sc and Ti on the one hand and Cr and Mn on the other hand would not be observed. But the scattered wave is scattered

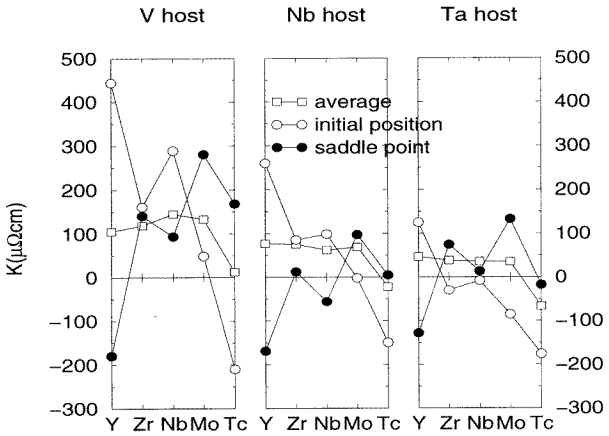

Figure 8. K for 4d impurities in V, Nb and Ta at the initial position and the saddle point, and the average over the path.

off the surrounding host atoms, giving rise to a wind force on the host atoms, which has already been observed as discussed in section 4, where the vacancy plays the role of the impurity. This wave, which has been scattered twice, is scattered again by the impurity, which gives a second contribution to the wind force on the impurity. The electrons scatter again and again, and all of these scattering events contribute to the final wind force. In the end, the wind force due to the first scattering event can be completely overshadowed.

5.2. Migration of the 4d impurities Y, Zr, Nb, Mo and Tc

The variation of K with respect to the atomic number is given in figure 8. Again K in the initial position and at the saddle point, and its path average are shown. One sees approximately the same features as for the 3d-impurity series of the previous subsection. The positive average wind valence is approximately constant with respect to the atomic number of the impurity, except for Tc, which even has a negative value in Nb and Ta. The wind valences are larger than the values for the 3d impurities, even the one of Nb in Nb. Still they are not very large and do not exceed the value of unity at high temperatures, where measurements can be performed. The wind valences at the initial position would decrease monotonically in all group VA hosts if the value of the impurity Zr were to be somewhat higher. The saddle-point value shows an increasing but oscillating trend. The low saddle-point value for the group VIIA impurity Tc was already observed for Mn.

This series of calculations shows a more consistent picture than the 3d series, in which the impurities interact with Nb differently to how they interact with V and Ta. In this series the variation of the values decreases with increasing atomic number of the host, and the trends for the saddle-point position as well as the initial position as functions of the atomic number of the impurity are similar in the three hosts. In view of the 3d calculations, it might be expected that impurities in a Nb host would behave differently. This is not the case and this is remarkable, because the host properties, calculated using the KKR method, which enter the calculation through $\mathcal{G}^{\mathrm{void}}$ and t^{h}, are not changed at all in calculations for different impurities.

The component of the force perpendicular to the migration path, characterized by $K_{\perp}$ as defined by equation (8), approximately follows the parallel component, characterized by

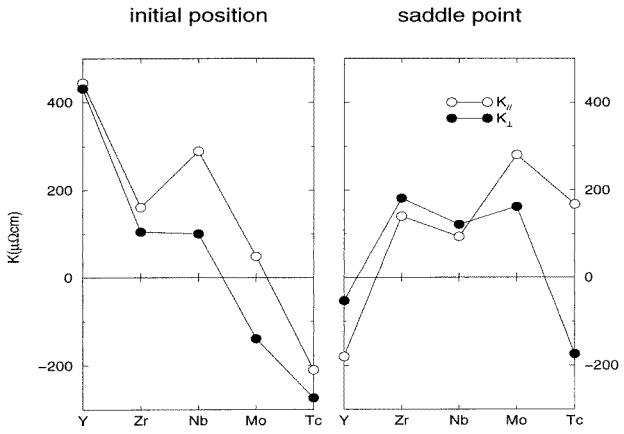

Figure 9. $K_{\parallel}$ and $K_{\perp}$ for 4d impurities in V at the initial position and at the saddle point.

$K_{\parallel}$ at the initial position. This is shown in figure 9 for V. $K_{\perp}$ is smaller, which is consistent with the picture of a ring current induced by the vacancy as proposed in subsection 5.1. The impurity Y hardly 'feels' any difference of $K_{\parallel}$ and $K_{\perp}$. At the saddle point, a different behaviour is observed, which is not very surprising. At the saddle point, the environment of the impurity has changed drastically. The nearest atoms (the six dark grey atoms in figure 1) are very close and the outcome of all backscattering effects is hard to predict. $K_{\parallel}$ can be either larger or smaller than $K_{\perp}$.

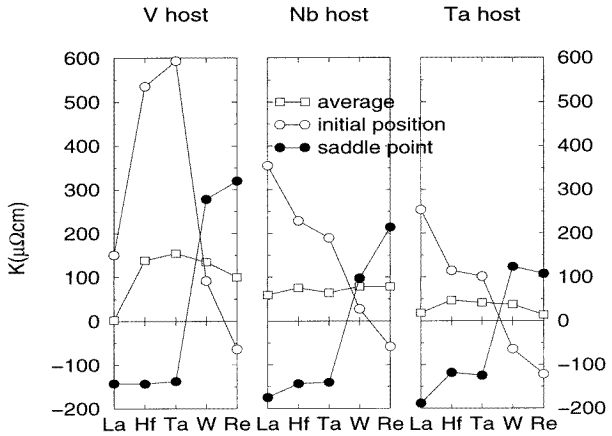

Figure 10. K for 5d impurities in V, Nb and Ta at the initial position and at the saddle point, and the average over the path.

5.3. Migration of the 5d impurities La, Hf, Ta, W and Re

In this series, the rare earths are not considered. Therefore the atomic number jumps from 57 for La to 72 for Hf. Similarly to the case for the 4d series, the path-averaged K-values decrease with increasing atomic number of the host, as is shown in figure 10. They also hardly vary with the atomic number of the impurity. The saddle-point value is negative

and of about the same magnitude for the impurities La, Hf and Ta in each of the three host metals. For W and Re, K at the saddle point is positive, the value for the group VIIA impurity Re being larger than those for W in V and Nb. In the 3d and 4d series, K for the group VIIA impurity at the saddle point is smaller, leading to a small path-averaged value. In this 5d series, the path-averaged K-value of Re is about the same size as those for the other 5d impurities. The values at the initial positions in Nb and Ta show monotonically decreasing trends as functions of the increasing atomic number. In V, this is not the case, and the maximum value is observed for Ta.

An overall view of the three series considered in the three group VA metals leads to the following observations. In general, the 3d impurities show the smallest path-averaged K, and the 5d impurities the largest. The trend for the host metals is reversed: K is largest for the 3d host metal V, while K is smallest for the 5d metal Ta. The path-averaged values within one series are in general equal for all impurities, but they result from completely different variations along the path. The saddle-point value increases with atomic number, whereas the initial-position value decreases. In the 3d as well as the 4d series, the group VIIA impurities have a separate position. They exhibit a smaller value of K as a result of a smaller value at the saddle point. For all impurities considered, the wind force turns out to be small—at most about 1. This makes these series suitable for measuring the direct valence, which is the dominant contribution to the measurable effective valence.

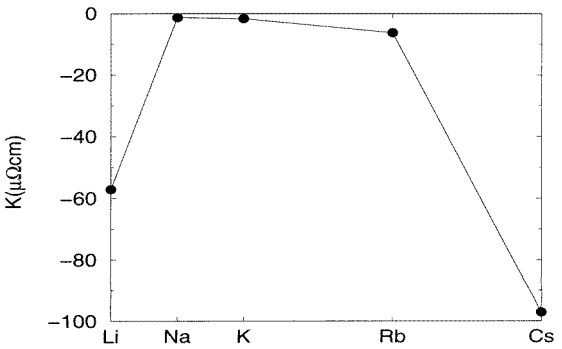

Figure 11. The average value of K for the alkali metals.

6. Results for other BCC metals

6.1. Self-electromigration in the alkali metals: Li, Na, K, Rb and Cs

The quantity K shows a sinusoidal variation as a function of the position along the migration path in the alkali metals. It varies from a small positive value at the initial position to a negative value at the saddle point, like in the noble metals [2]. The average values are negative for all alkali metals, as shown in figure 11. K for Li and Cs is considerably larger in magnitude than K for Na, K and Rb.

Measurements have been performed on self-electromigration in Li [23] and Na [24]. Using equation (9), a direct valence of 1.2 and a K-value of $-35\ \mu\Omega$ cm correspond to the variation of the effective valence from -1.8 at 363 K to -1.2 at 433 K in Li. This K-value is in reasonable agreement with the theoretical value of $-57\ \mu\Omega$ cm. The measured direct valence indicates an unscreened charge. The experimental effective valence found for Na

is of the same order of magnitude as that found for Li and cannot be explained by our calculations.

Table 4. The wind valence for self-electromigration and the resistivity at $0.9T_m$ for Ca, Sr and Ba, and T_m.

	$Z_{wind}(0.9T_m)$	$\rho(0.9T_m)$ ($\mu\Omega$ cm)	T_m
Ca	5.4	13	1112
Sr	0.5	52	1041
Ba	0.9	188	985

6.2. Self-electromigration in the group IIA metals: Ca, Sr and Ba

Of the group IIA metals, Ba has a BCC lattice structure at all temperatures below the melting temperature, while Ca and Sr are FCC metals at low temperatures, but undergo a structural phase transition to BCC metals at elevated temperatures. The resistivity grows quickly as a function of atomic number as can be seen from table 4. The wind valence at 0.9 T_m, given in that table, is large for Ca, whereas for Ba and Sr it is much smaller. To our knowledge, no electromigration measurements have been made for these metals. They would be very hard to perform, because of the high reactivity with hydrogen.

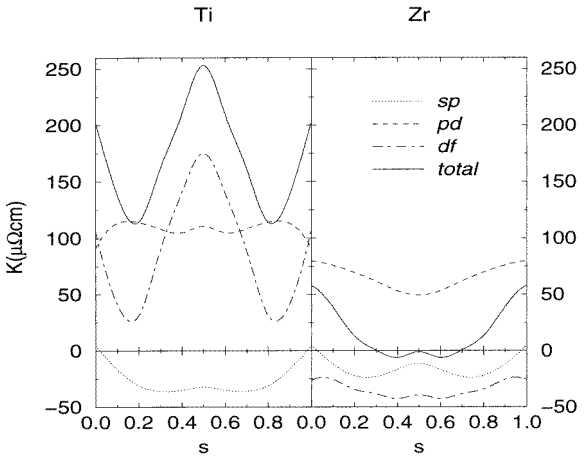

Figure 12. The variations of K^{sp}, K^{pd}, K^{df} and K along a path in Ti and Zr with the BCC structure.

6.3. Self-electromigration in the group IVA metals: Ti and Zr

In figure 12 the variations of the three contributions to K along a path in Ti and Zr are shown. Notwithstanding their electronic similarity, the variations of the angular momentum components along the path differ. The sp contributions to K are similar and the magnitudes of the pd contributions are comparable, but they vary differently though not very much. The df contributions show a completely different behaviour. The df contribution in Ti is large and positive and shows large variations. In Zr it is much smaller, negative and

approximately constant and, together with the sp component, it almost cancels the positive pd component. This leads to a wind force which is much smaller in magnitude than each of its components.

The average K-value of Ti of 169.2 $\mu\Omega$ cm is an order of magnitude larger than that of Zr (14.9 $\mu\Omega$ cm). The latter is small—similarly to what was found for the close-packed 4d metals [2]. At a temperature of 1900 K, the wind valences of Ti and Zr are 1.05 and 0.12 respectively.

These metals belong to the group of so-called anomalous BCC metals, in which a remarkable temperature dependence of the diffusion constant is observed. This is commonly attributed to the presence of different diffusion mechanisms. In order to get more information about these mechanisms, electromigration experiments have been carried out. Campbell and Huntington [25] performed measurements on Zr and Dübler and Wever [26] on both Ti and Zr. The measurements are complicated by thermomigration, which is an atomic migration effect in the presence of temperature gradients. Electromigration and thermomigration effects are hard to separate if the thermomigration is relatively large. As a result of this, the effective valence is not accurately known, but it is certainly smaller than one. The small positive value for Zr is in agreement with the experiments if the direct valence is assumed to be zero. Dübler and Wever state that the monovacancy mechanism, which is used in our calculations, is not very likely to be observed in their measurements for Ti.

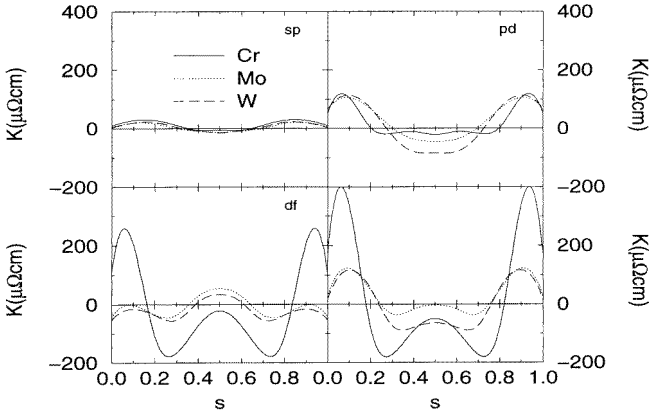

Figure 13. The variations of K^{sp}, K^{pd}, K^{df} and K along a path in the group VIA metals Cr, Mo and W.

6.4. Self-electromigration in the group VIA metals: Cr, Mo and W

In figure 13, the variations of the three different angular momentum contributions to K and their sum is given for the three group VIA metals Cr, Mo and W. It is to be noticed that the antiferromagnetic ordering in Cr has vanished at high temperatures, at which electromigration measurements are performed. Therefore a paramagnetic calculation is justified. Similarly to the case of the group VA metals, an initially increasing positive wind valence is seen, after which a decrease follows. After the decrease, a new increase follows, which is not observed for the group VA metals, and a local maximum is reached at the saddle point. The variation of K is much larger for Cr than for the other two metals. The deviant behaviour of Cr is mostly a result of the df contribution. The sp contribution is

small for all group VIA metals, while the pd term shows a similar variation for the three metals, although the maximum for Cr is reached more quickly than those for Mo and W. The average K for all of the metals is positive, although it is very small for W, namely 2.0 $\mu\Omega$ cm, whereas the resistivity at 2500 K is about 73 $\mu\Omega$ cm. K has the same order of magnitude for Cr and Mo; that is, $K = 24.4$ $\mu\Omega$ cm for Cr and $K = 30.0$ $\mu\Omega$ cm for Mo.

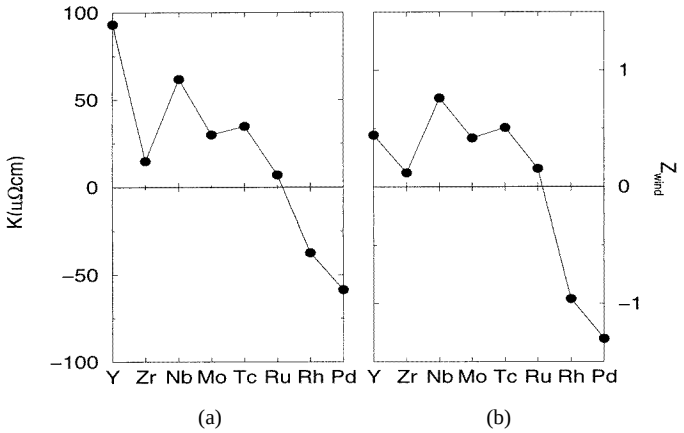

Figure 14. K and Z_{wind} (at $0.9T_{\mathrm{m}}$) for all 4d transition metals, where the calculations for the metals with a close-packed lattice structure were carried out previously [2].

By now, results for self-electromigration in *all* 4d metals are available, because in a previous publication the 4d metals with a close-packed lattice structure were considered [27, 2]. The average K-values for these calculations together with those for Zr (section 6.3), Nb (section 3) and Mo are shown in figure 14(a). Z_{wind}-values at 90% of the melting temperature for each metal are shown in figure 14(b). The relatively small value of K for Zr disturbs the decreasing trend with increasing atomic number. This path-averaged K is the result of strong variations along the path, which are quite different for the different metals, and it is surprising that in spite of this such a trend is observed.

7. Summary

The application of a recently developed *ab initio* KKR Green's function theory [2] is extended to a number of BCC metals. The overall negative wind valence for self-electromigration in the alkali metals Li, Na, K, Rb and Cs shows a strange behaviour as a function of atomic number. The values for Li and Cs are much larger in magnitude than the ones for Na, K and Rb. The calculated wind valence in Li in good agreement with experiment [23], while that in Na is not [24]. For the group IIA metals, no clear trend is observed in spite of their electronic similarity. The anomalous BCC metals Ti and Zr, where 'anomalous' refers to the temperature dependence of the diffusion constant, show a remarkably varying wind valence along the path, similar to what was already observed for transition metals with the FCC structure. The calculated wind valence in Zr is in agreement with experiment, if a zero direct force is assumed.

Self-electromigration in the group VA metals V, Nb and Ta is treated more extensively. Different authors have [11, 18] reported different measured values of the effective valence in Nb. Both measurements can be made to agree with our calculation by assuming a different value of the direct valence. Comparison of our results with other calculations, which neglect

either backscattering [11] or the electronic structure of the host [15], shows the importance of both effects.

The role of the vacancy as regards the wind force at the initial position is investigated for V. Charge transfer from the host atom to the vacancy plays a role. The perturbed atom interacts with the sample current, which gives a contribution to the wind force. Calculation of the wind force on an atom at different positions with respect to the vacancy and the electric field suggests that the vacancy induces a ring current, which is scattered by the atom.

A similar effect of the vacancy is seen in impurity migration in the group VA metals. Furthermore, a decreasing value as a function of the atomic number at the initial position is compensated by an increasing value at the saddle point for 3d, 4d and 5d impurities in V, Nb and Ta. The average wind valences for the transition metal impurities are small. Therefore, these series can be useful in the study of the direct force.

The wind valences for self-migrating group VIA atoms are small, as is observed for most transition metals. Together with earlier calculations of the wind force in close-packed 4d metals [2], the calculations for Zr, Nb and Mo complete the series for all 4d transition metals. Apart from for Zr, K decreases as a function of atomic number. The wind valence shows a similar trend, although that of Y is relatively low.

Acknowledgments

This work was sponsored by the National Computing Facilities Foundation (NCF) as regards the use of supercomputer facilities, supported financially by the Nederlandse Organisatie voor Wetenschappelijk Onderzoek (Netherlands Organization for Scientific Research, NWO).

The authors wish to thank Mr P J Harte for making the calculations of the wind force reliable over the region of the path between 5% and 15% of the path length away from the initial position.

References

[1] Ho P S and Kwok T 1989 *Rep. Prog. Phys.* **52** 301
[2] Dekker J P, Lodder A and van Ek J 1997 *Phys. Rev.* B **56** 12 167
[3] Lodder A 1984 *J. Phys. F: Met. Phys.* **14** 2943
[4] Lodder A 1976 *J. Phys. F: Met. Phys.* **6** 1885
[5] Korringa J 1947 *Physica* **13** 392
[6] Kohn W and Rostoker N 1954 *Phys. Rev.* **94** 1111
[7] Sorbello R S, Lodder A and Hoving S J 1982 *Phys. Rev.* B **25** 6178
[8] Bosvieux C and Friedel J 1962 *J. Phys. Chem. Solids* **23** 123
[9] Sorbello R S 1973 *J. Phys. Chem. Solids* **34** 937
[10] Gupta R P 1982 *Phys. Rev.* B **25** 5188
[11] Gupta R P, Serruys Y, Brebec G and Adda Y 1983 *Phys. Rev.* B **27** 672
[12] Dekker J P, Lodder A, Zeller R and Tatarchenko A F 1996 *Phys. Rev.* B **54** 4531
[13] Lodder A and Dekker J P 1997 *Properties of Complex Inorganic Solids; Proc. 1st Int. Alloy Conf. (Athens, Greece, 1996)* ed A Gonis, A Meike and P E A Turchi (New York: Plenum) p 467
[14] Lodder A and Brand M G E 1984 *J. Phys. F: Met. Phys.* **14** 2955
[15] Brand M G E and Lodder A 1986 *Phys. Status Solidi* b **133** 119
[16] van Ek J and Lodder A 1991 *J. Phys.: Condens. Matter* **3** 7331
[17] van Ek J and Lodder A 1991 *J. Phys.: Condens. Matter* **3** 8403
[18] Ernst B, Frohberg G and Wever H 1997 *Defect Diffusion Forum* **143–147** 1655
[19] Pines D and Nozières 1966 *The Theory of Quantum Liquids* (New York: Benjamin)
[20] Landauer R 1957 *IBM J. Res. Dev.* **1** 223

[21] Sorbello R S 1981 *Phys. Rev.* B **23** 5119
[22] Lodder A and Dekker J P 1998 *Stress Induced Phenomena in Metallization; 4th Int. Workshop (Tokyo, 1997)* ed H Okabayashi, S Shingubara and P S Ho (Woodbury, NY: American Institute of Physics) p 315
[23] Thernquist P and Lodding A 1968 *Z. Naturf.* a **23** 627
[24] Sullivan G A 1967 *Phys. Rev.* **154** 605
[25] Campbell D R and Huntington H B 1969 *Phys. Rev.* **179** 601
[26] Dübler H and Wever H 1968 *Phys. Status Solidi* **25** 109
[27] Dekker J P and Lodder A 1997 *Defect Diffusion Forum* **143–147** 1645